

Calculation of Rotor Performance and Loads Under Stalled Conditions

Hyeonsoo Yeo
hsyeo@mail.arc.nasa.gov

Raytheon ITSS
Army/NASA Rotorcraft Division
NASA Ames Research Center
Moffett Field, California

Abstract

Rotor behavior in stalled conditions is investigated using wind tunnel test data of a 1/10-scale CH-47B/C type rotor, which provides a set of test conditions extending from unstalled to light stall to some deep stall conditions over a wide range of advance ratios. The rotor performance measured in the wind tunnel is similar to the main rotor performance measured during the NASA/Army UH-60A Airloads Program, although the two rotors are quite different. The analysis CAMRAD II has been used to predict the rotor performance and loads. Full-scale airfoil test data are corrected for Reynolds number effects for comparison with the model-scale rotor test. The calculated power coefficient shows good correlation with the measurements below stall with the Reynolds number-corrected airfoil table. Various dynamic stall models are used in the calculations. The Boeing model shows the lift augmentation at low advance ratios and the Leishman-Beddoes model shows better correlation of torsion moment than the other models at $\mu = 0.2$. However, the dynamic stall models, in general, show only a small influence on the rotor power and torsion moment predictions especially at higher advance ratios.

Introduction

Many rotor components and fixed-system controls are sized by the loads in maneuvers. Often, these design loads are scaled from flight test data bases, as calculations are not trustworthy. To a substantial degree, the limitations of analysis are caused by the inability to predict rotor stall, including the effects of dynamic stall. Dynamic stall is a phenomenon where a vortex is shed near the leading edge of an airfoil and increases the lift as the vortex passes along the upper surface, but also increases moment (thus control loads) and drag.

Dynamic stall for 2-D conditions has been studied for many years both experimentally and analytically. Numerous wind tunnel experiments of oscillating airfoils have been conducted to better understand the phenomenon [1-5]. Many semi-empirical dynamic stall models have been developed, based on measured c_l , c_m , and c_d loops, to predict the effects of dynamic stall [6-10] and in many cases these semi-empirical models provide a good match to oscillating 2-D airfoil test data [11]. Although these semi-empirical models

Notation

C_L/σ	rotor lift coefficient
C_p/σ	rotor power coefficient
C_{pi}/σ	rotor induced power coefficient
C_{po}/σ	rotor profile power coefficient
C_w/σ	gross weight coefficient
d	rotor diameter
M	Mach number
q	dynamic pressure
R	rotor radius
X	rotor propulsive force
α	angle of attack
μ	advance ratio
σ	solidity

Presented at the American Helicopter Society 59th Annual Forum, Phoenix, Arizona, May 6-8, 2003. Copyright © 2003 by the American Helicopter Society International, Inc. All rights reserved.

have been integrated into comprehensive analyses, comparatively little effort has given to the evaluation of the comprehensive codes' capability to predict rotor behavior under stalled conditions. References 12 and 13 compared the calculated blade loads with the flight test data from an UH-60A Airloads Program [14] at $C_w/\sigma = 0.13$ and $\mu = 0.23$. In general, the correlation was not satisfactory for any of the semi-empirical models examined.

Recent performance analysis of a utility helicopter has shown that the calculated power coefficient generally agrees well with flight test data [15]. However, the accuracy of the calculation degrades at high gross weight and the use of a semi-empirical dynamic stall model does not improve the correlation.

It is important to understand the changes in rotor performance and trim as a blade becomes stalled. This problem is easily examined for wind tunnel conditions compared to flight conditions. Wind tunnel test data obtained by McHugh and his colleagues [16-18] provide a set of test conditions extending from unstalled to light stall to some deep stall conditions over a wide range of advance ratios and are a useful intermediate step between 2-D wind tunnel tests and flight data. The objective of the test was to define the lift and propulsive force limits of a conventional rotor and examine performance, control power, and blade loads near these limits. These extensive test data sets provide a useful resource that can be used to examine the rotor behavior in the stalled condition.

The purpose of this study is threefold: 1) assess the suitability of the McHugh wind tunnel test data, 2) carry out comprehensive calculations using CAMRAD II with various dynamic stall models and compare the results with the test data, and 3) evaluate various dynamic stall models and identify or suggest important elements that are needed to obtain improved correlation.

Wind Tunnel Test Data

The McHugh wind tunnel test was conducted in the 20-by 20-foot test section of the Boeing Vertol V/STOL Wind Tunnel. The test was performed with a 1/10-scale CH-47B/C type rotor which has a V23010-1.58 airfoil section and a linear twist of -7 degrees. The rotor was designed with sufficient structural strength that the true aerodynamic limits were obtained. The model blade had a -3 degree trailing edge tab angle (deflected 3 degrees up). The blade physical properties are summarized in Table 1.

In the wind tunnel test, a sweep in rotor lift coefficient was made at a fixed rotor propulsive force coefficient

by increasing shaft angle and collective at the required advance ratio and advancing tip Mach number [17]. A total loads balance was used to measure six components of force and moment. Rotor control positions and blade flap and chord bending and torsion moments were also measured.

CAMRAD II Analysis

Performance calculations were carried out using the comprehensive rotorcraft analysis CAMRAD II [19]. Six beam elements were used in modeling the main rotor blade and 18 aerodynamic segments were used for the aerodynamic calculation. A 15-deg azimuthal resolution was used for the analysis. The trim solution solves for the shaft angle and cyclic controls to achieve the specified propulsive force and zero 1/rev longitudinal and lateral flapping angles at a given collective. Performance was calculated using nonuniform inflow with free wake geometry and unsteady aerodynamics (ONERA EDLIN model). Five dynamic stall models available in CAMRAD II were used in the calculations. Those five models are the Johnson [7], Boeing [6], Leishman-Beddoes [8], ONERA EDLIN (Equations Differentielles Lineaires) [9], and ONERA BH (Bifurcation de Hopf) [10] models.

The five dynamic stall models require empirical parameters derived either from static stall characteristics or oscillating airfoil tests. The dynamic stall parameters used in the current analysis are typical values for a NACA 0012 airfoil. For the Leishman-Beddoes model, four parameters were derived from the static stall characteristics of the V23010-1.58 airfoil. These four parameters are: α_s , s_1 , and s_2 which define the trailing edge separation function f , and the critical lift coefficient

Table 1 Rotor Blade Properties [17]

Airfoil	V23010-1.58
Radius	2.9583 ft
Chord	0.1913 ft
Flap hinge offset	2.12 in.
Pitch axis location	25% chord
Blade twist	-7 degree (linear)
Number of blades	3
Lock number	6.7
Solidity	0.06175
Flap inertia	0.0319 slug-ft ²
Weight inertia	0.516 ft-lb

at the separation onset boundary (c_l at $f = 0.7$).

$$f = \begin{cases} 1 - 0.3 \exp\{(\alpha - \alpha_s)/s_1\} & \text{if } \alpha \leq \alpha_s \\ 0.04 + 0.66 \exp\{(\alpha_s - \alpha)/s_2\} & \text{if } \alpha > \alpha_s \end{cases}$$

where α_s defines the breakpoint corresponding to $f = 0.7$ and the coefficients s_1 and s_2 define the static stall characteristics. Reference 20 provides details of the dynamic stall models implemented in CAMRAD II.

Assessment of Wind Tunnel Test Data

An assessment of the wind tunnel test data was made to identify the suitability of the data for the evaluation of the analytical tool.

Figure 1, from Ref. 17, shows the maximum lift limit measured from the wind tunnel test for $X/qd^2\sigma = 0.05$, where X is propulsive force, q is dynamic pressure, d is rotor diameter, and σ is rotor solidity. McHugh defined two limits in Ref. 17: "without tip stall" and "with tip stall" cases. However, no detailed explanation was provided about the criteria for defining the two cases. The circles and solid faired line represent the "without tip stall" case and the squares and dashed faired line the "tip stall case." The only values used in Ref. 16 are non-tip stall case. It should be noted that the lift limit at $\mu = 0$ was defined by the maximum collective pitch attainable with the normal length pitch links. For the high speed testing, a set of long pitch links was used but no hover data were obtained [17].

The repeatability of the test data has been examined. Figure 2 shows the rotor lift coefficient versus rotor power coefficient for four advance ratios [18]. These are the only repeat test cases available. Test conditions for these data are: $X/qd^2\sigma = 0.05$ and $V_{TIP} = 620$ ft/sec. Significant differences between the data sets are observed at a number of advance ratios. Some of the observed differences occur at low to moderate advance ratios where little or no stall occurs on the rotor. The reasons for the observed differences are not known at present.

Airfoil Characteristics

A 2D airfoil table in C81 format was constructed from aerodynamic characteristics of the V23010-1.58 airfoil with a -3 deg trailing-edge tab in Ref. 21. The airfoil test data were obtained at full-scale Reynolds numbers.

For comparison with model-scale data, it is necessary to correct full-scale airfoil test data for Reynolds number

effects. The Reynolds number correction on drag was made based on the following equation.

$$C_{dFS} = C_{dMS} \left(\frac{Re_{MS}}{Re_{FS}} \right)^{0.14} \quad (1)$$

where FS and MS are full-scale and model-scale respectively. The exponent 0.14 was derived from the relationship proposed by McCroskey [22] which is based on the most trustworthy NACA 0012 airfoil characteristics obtained from more than 40 wind tunnel tests. This relationship is:

$$c_{d0} = 0.0044 + 0.018 Re^{-0.15} \quad (2)$$

For the CH-47B/C model rotor, this change increases drag by 38% at all angles of attack and Mach numbers. It should be noted that Ref. 23 recommended that the exponent of Eq. 1 should be 0.2 based on the turbulent drag trends and Ref. 24 recommended values between 0.12 and 0.2.

Reference 22 also showed the variation of $c_{l_{max}}$ as a function of Reynolds number, which is valid at Mach numbers below 0.25. In Ref. 22, the $c_{l_{max}}$ is reduced by 26.4% for a Reynolds number change from 10^7 to 10^6 . For the present study, it is assumed that the reduction of $c_{l_{max}}$ is 26.4% at $M = 0.2$, the reduction decreases linearly, and there is no change in $c_{l_{max}}$ at $M = 0.6$, where a true maximum lift is not defined. Lift slope also changes according to Reynolds number [22]. However, the change is very small (less than 5%) and was neglected in the current study.

A Reynolds number correction for moment was made consistent with that used for lift by adjusting the moment based on the changes in the stall angle of attack. It is noted that Ref. 23 has also shown a reduction of the static stall angle of attack for both lift and moment as Reynolds number is reduced.

Figure 3 shows the lift, drag, and moment coefficients of the full-scale and model-scale airfoils at three Mach numbers. The reference chord line is defined such that it bisects the aft 50 percent of the airfoil profile [21]. The Reynolds number-corrected airfoil characteristics are shown in Fig. 3 along with the full-scale characteristics.

Results and Discussion

Blade Natural Frequency

The frequency spectrum for the model blade in Ref. 17 was estimated from structural response data obtained

while rotor speed was varied from 1100 to 2100 rpm. The forward flight airloads were used to excite the blade motion. The frequencies of these airloads are N/rev , where $N = 1, 2, \dots$, regardless of the rotor speed. As the rotor speed varies, the blade responds to the airloads and a large response is observed when resonance occurs. This technique, however, can only be used to identify lower-damped, higher-frequency modes.

For the analytical calculations, it was necessary to develop an approximate model of the 1/10-scale model rotor as there are no detailed structural properties for the model blade available. Full-scale CH-47B blade properties were obtained from the Boeing Company and were scaled to the model configuration and further adjustments were made to match the measured model blade weight moment, flap inertia, and frequencies.

The calculated blade natural frequencies are compared with measurements in Fig. 4. The analysis shows fair to good agreement with the measurements at 3rd flap, 4th flap, and 2nd lag modes. The difference between measurements and analysis appears at 1st torsion and 3rd lag modes. The measurements show that the torsion frequency increases with rotor speed and the 3rd lag frequency is just above the 4th flap frequency. The analysis shows that the torsion frequency is insensitive to the rotor speed and does not show the 3rd lag mode. The reasons for these differences are not known.

Effects of Reynolds Number on Calculated Performance

Rotor performance was calculated with CAMRAD II using both the full-scale and the Reynolds number-corrected airfoil decks. These calculations are compared with measurements at four different advance ratios for $X/qd^2\sigma = 0.05$ as shown in Fig. 5. The measured main rotor power of a UH-60A Black Hawk obtained in the NASA/Army UH-60A Airloads Program [15] is also shown. The comparison between the wind tunnel test and flight test data will be discussed below.

Figure 5 shows the rotor lift versus the sum of rotor induced power and profile power. The equivalent rotor drag can be calculated by dividing rotor induced plus profile power by airspeed. Thus this figure provides information equivalent to a maneuver lift-drag polar. Wind tunnel test data show a moderate increase in the rotor induced plus profile power without stall. As stall becomes important, then the slope of the power curve quickly flattens. The maximum lift capability of the rotor decreases as the advance ratio increases.

For the CAMRAD II calculations, the collective angle is progressively increased up to and through stall. In these

calculations, a free wake and unsteady aerodynamics were used, but a dynamic stall model was not incorporated. The calculated power coefficient shows good correlation with the measurements below stall with the Reynolds number-corrected airfoil table except at $\mu = 0.1$, where the analysis underpredicts the power at all lift levels. The analysis shows good correlation with Run 28 data at $\mu = 0.2$. The Reynolds number correction on drag increases the rotor power and the power increase is larger at higher advance ratios. The effect of Reynolds number correction on lift appears as the rotor blade experiences stall. The rotor lift coefficient decreases with the Reynolds number-corrected airfoil at high lift conditions, thus the correlation is improved.

The measured main rotor power of a UH-60A Black Hawk obtained in the NASA/Army UH-60A Airloads Program is compared with McHugh wind tunnel test data in Fig. 5. Although there are significant differences between the two rotors and in the test conditions, the two data sets are quite similar. Good agreement is observed at the advance ratios of 0.1 and 0.2. This comparison also shows that the Run 28 data set provides a better representation of power measurement at $\mu = 0.2$. Differences appear between the two data sets at the advance ratio of 0.3. The possible reasons are: Reynolds number, airfoil characteristics, blade twist, propulsive force, etc. The two rotors experience stall at the almost same level of lift.

Effects of Dynamic Stall on Performance and Loads

Calculations with dynamic stall models were made to assess the increments in the prediction of the rotor performance and loads and the results are compared with measurements at four different advance ratios as shown in Figs. 6 through 8.

Figure 6 shows the rotor lift versus rotor induced plus profile power. Calculations have been made using all the five dynamic stall models available in CAMRAD II. However, only results with three dynamic stall models (Boeing, Leishman-Beddoes, and ONERA-BH) are presented along with the baseline (without dynamic stall model) result. The Boeing model shows lift augmentation at the advance ratios of 0.1 and 0.2. However, the model does not show any significant changes from the baseline result at the advance ratios of 0.3 and 0.4. The Leishman-Beddoes model shows little difference from the baseline at all advance ratios. Unlike 2-D dynamic stall characteristics, the rotor lift is slightly decreased at $\mu = 0.2$. A converged solution was not achieved with the Leishman-Beddoes model at $\mu = 0.4$ and $C_L/\sigma \geq 0.08$. The ONERA-BH model also shows little difference from the baseline results. A converged solution was not achieved with this model at earlier lift

levels than the Leishman-Beddoes model. Although not shown here, the Johnson model showed similar results as the Boeing model and the ONERA-EDLIN model showed convergence problems earlier than the ONERA-BH model.

Rotor control angle results at $\mu = 0.2$ are examined in Fig. 7. The test data show that there is good agreement in collective and lateral cyclic angles between the two test runs (Runs 27 and 28), considering the scatter of the measured data. However, the longitudinal cyclic angles are quite different and this difference may result in the difference in the rotor power (Fig. 5). For the same collective angle, the Boeing model increases the rotor lift but both the Leishman-Beddoes and the ONERA-BH models slightly decrease the rotor lift. The analysis overpredicts the longitudinal cyclic and underpredicts the lateral cyclic. The measurements show that the lateral cyclic angles increase moderately as the rotor lift increases. However, the analysis shows a rather sharp increase near the lift limit. When the collective angle was further increased, both the Boeing and the Leishman-Beddoes models show a significant increase of the lateral cyclic angle.

Figure 8 shows alternating torsion moment at 11.8% radius. Oscillating 2-D airfoil test data show a significant increase in nose-down pitching moments as the leading-edge vortex convects downstream along the airfoil upper surface and this results in large control loads. Since pitch link loads are not available, the torsion moment measured at the most inboard section of the blade is examined. The measurement shows a significant increase in the torsion moment as the rotor experiences stall. The analysis underpredicts the torsion moment below stall at all speeds. The analysis, in general, captures the trends at the advance ratios of 0.1 and 0.2. The Boeing model shows a greater increase in the rotor lift than in the torsion moment. Both the Leishman-Beddoes and ONERA-BH models show a slight moment increase at $\mu = 0.1$. The Leishman-Beddoes model shows better correlation than the other models at $\mu = 0.2$. The analysis, however, is not able to capture the significant moment increase near the rotor lift limit at the advance ratios of 0.3 and 0.4, although the analysis was more successful in capturing the power increase as shown in Fig. 6.

Effect of Time Step on the Dynamic Stall Calculation

The effect of time steps on the performance and loads calculation is examined using the Leishman-Beddoes model. It is necessary to examine whether the 15 deg time step used in the current analysis has enough azimuthal resolution to capture the dynamic stall phenomenon, which is known to occur within a short time period.

Figure 9 shows the rotor performance and torsion moment at the advance ratio of 0.2. In this calculation, 15, 10, and 5 deg time steps are used. As expected, the time step does not change results below stall. The higher azimuthal resolution increases the rotor lift near the lift limit and improves the performance correlation. However, the calculation shows that the azimuthal step change has a small influence on the rotor power and torsion moment for the same trim values.

Conclusions

Rotor behavior in stalled conditions has been examined using the McHugh wind tunnel test of a 1/10-scale CH-47B/C type rotor. The analysis CAMRAD II has been used to predict the rotor performance and loads using various dynamic stall models.

Considering the adequacy of the test data, the following conclusions are obtained:

1. An examination of the repeatability of the test data has shown significant differences between the data sets for the same test conditions at a number of advance ratios. However, the reasons for the differences are not known at present.
2. The absence of detailed structural properties for the model blade has reduced the utility of the test data.
3. A comparison between the McHugh wind tunnel and the UH-60A Airloads Program flight performance data shows good agreement at lower advance ratios, although the two rotors are quite different. This comparison shows that the Run 28 data set provides better representation of power measurement at $\mu = 0.2$.

The analysis CAMRAD II has been used to correlate with the McHugh test data and the following conclusions are obtained:

1. The calculated power coefficient using CAMRAD II shows good correlation with the measurements below stall with the Reynolds number-corrected airfoil table except at $\mu = 0.1$, where the analysis underpredicts the power at all lift levels. Maximum lift is well predicted using Reynolds number-corrected static stall characteristics.
2. For calculations using semi-empirical dynamic stall models, the Boeing model shows the lift augmentation at low advance ratios and the Leishman-Beddoes model shows better correlation

of torsion moment than the other models at $\mu = 0.2$. However, the dynamic stall models, in general, show a small influence on the rotor power and torsion moment predictions especially at higher advance ratios.

3. Convergence problems occur at high advance ratios and the inclusion of dynamic stall models exacerbates convergence issues due to strong nonlinearities.
4. An examination of the effect of time steps on the performance and loads calculation using the Leishman-Beddoes model shows that the higher azimuthal resolution increases the rotor lift near the lift limit but the azimuthal resolution change has a small influence on the rotor power and torsion moment for the same trim values.

Recommendation

A new wind tunnel test is required to better understand the effects of stall on the rotor performance and loads and to provide more complete benchmark data sets for the evaluation of analyses. The test should consider the following factors: careful documentation of blade structural properties, airfoil characteristics at proper Reynolds number, measurement of blade airloads, and measurement of rotor stability.

Acknowledgment

The authors would like to express thanks to Bobby Mathew, Frank Tarzanin, and Leo Dadone at the Boeing Company for sharing their valuable data and knowledge.

References

- [1] Liiva, J., and Davenport, F. J., "Dynamic Stall of Airfoil Sections for High-Speed Rotors," *Journal of the American Helicopter Society*, Vol. 14, No. 2, April 1969.
- [2] Martin, J. M., Empey, R. W., McCroskey, W. J., and Caradonna, F. X., "An Experimental Analysis of Dynamic Stall on an Oscillating Airfoil," *Journal of the American Helicopter Society*, Vol. 19, No. 1, January 1974.
- [3] Dadone, L. U., "Two-Dimensional Wind Tunnel Test of an Oscillating Rotor Airfoil, Volume I," NASA CR 2915, December 1977.
- [4] McCroskey, W. J., McAlister, L. W., Carr, L. W., and Pucci, S. L., "An Experimental Study of Dynamic Stall on Advanced Airfoil Sections Volume 1. Summary of Experiments," NASA TM 84245, July 1982.
- [5] Piziali, R. A., "2-D and 3-D Oscillating Wing Aerodynamics for a Range of Angles of Attack Including Stall," NASA TM 4532, USAATCOM TR 94-A-011, September 1994.
- [6] Gormont, R. E., "A Mathematical Model of Unsteady Aerodynamics and Radial Flow for Application to Helicopter Rotors," USAAVLABS TR 72-67, May 1973.
- [7] Johnson, W., "The Response and Airloading of Helicopter Rotor Blades Due to Dynamic Stall," ASRL TR 130-1, May 1970.
- [8] Leishman, J. G., and Beddoes, T. S., "A Semi-Empirical Model for Dynamic Stall," *Journal of the American Helicopter Society*, Vol. 23, No.3, July 1989.
- [9] Petot, D., "Differential Equation Modeling of Dynamic Stall," La Recherche Aerospaciale, Number 1989-5 (corrections dated October 1990).
- [10] Truong, V. K., "A 2-D Dynamic Stall Model Based on a Hopf Bifurcation," Nineteenth European Rotorcraft Forum, Marseilles, France, September 1998.
- [11] Tan, C. M., and Carr, L. W., "The AFDD International Dynamic Stall Workshop on Correlation of Dynamics Stall Models with 3-D Dynamic Stall Data," NASA TM 110375, July 1996.
- [12] Nguyen, K., and Johnson, W., "Evaluation of Dynamic Stall Models with Uh-60A Airloads Flight Test Data," American Helicopter Society 54th Annual Forum Proceedings, May 1998.
- [13] Kufeld, R. M., and Johnson, W., "The Effects of Control System Stiffness Models on the Dynamics Stall Behavior of a Helicopter," *Journal of the American Helicopter Society*, Vol. 45, No. 4, October 2000.
- [14] Kufeld, R. M., Balough, D. L., Cross, J. L., Studebaker, K. F., Jennison, C. D., and Bousman, W. G., "Flight Testing of the UH-60A Airloads Aircraft," American Helicopter Society 50th Annual Forum Proceedings, Washington D.C., May 1994.

- [15] Yeo, H., Bousman, W. G., and Johnson, W., "Performance Analysis of a Utility Helicopter with Standard and Advanced Rotors," American Helicopter Society Aerodynamics, Acoustics, and Test and Evaluation Technical Specialist Meeting Proceedings, San Francisco, California, January 2002.
- [16] McHugh, F. J., "What Are The Lift and Propulsive Force Limits At High Speed For The Conventional Rotor?," American Helicopter Society 34th Annual Forum Proceedings, May 1978.
- [17] McHugh, F. J., Clark, R., and Solomon, M., "Wind Tunnel Investigation of Rotor Lift and Propulsive Force at High Speed - Data Analysis," NASA CR 145217-1, October 1977.
- [18] McHugh, F. J., Clark, R., and Solomon, M., "Wind Tunnel Investigation of Rotor Lift and Propulsive Force at High Speed - Test Data Appendix," NASA CR 145217-2, October 1977.
- [19] Johnson, W., "Technology Drivers in the Development of CAMRAD II," American Helicopter Society Aeromechanics Specialist Meeting, San Francisco, California, January 1994.
- [20] Johnson, W., "Rotorcraft Aerodynamics Models for a Comprehensive Analysis," American Helicopter Society 54th Annual Forum Proceedings, Washington, D.C., May 1998.
- [21] Dadone, L. U., "U.S. Army Helicopter Design DATCOM, Volume I - Airfoils," Boeing Doc. No. D210-11097-1, May 1976.
- [22] McCroskey, W. J., "A Critical Assessment of Wind Tunnel Results for the NACA 0012 Airfoil," NASA TM 100019, October 1987.
- [23] Keys, C. N., McVeigh, M. A., Dadone, L., and McHugh, F. J., "Estimation of Full-Scale Rotor Performance from Model Rotor Test Data," American Helicopter Society 39th Annual Forum Proceedings, May 1983.
- [24] Yamauchi, G. K., and Johnson, W., "Trends of Reynolds Number Effects on Two-Dimensional Airfoil Characteristics for Helicopter Rotor Analyses," NASA TM 84363, April 1983.

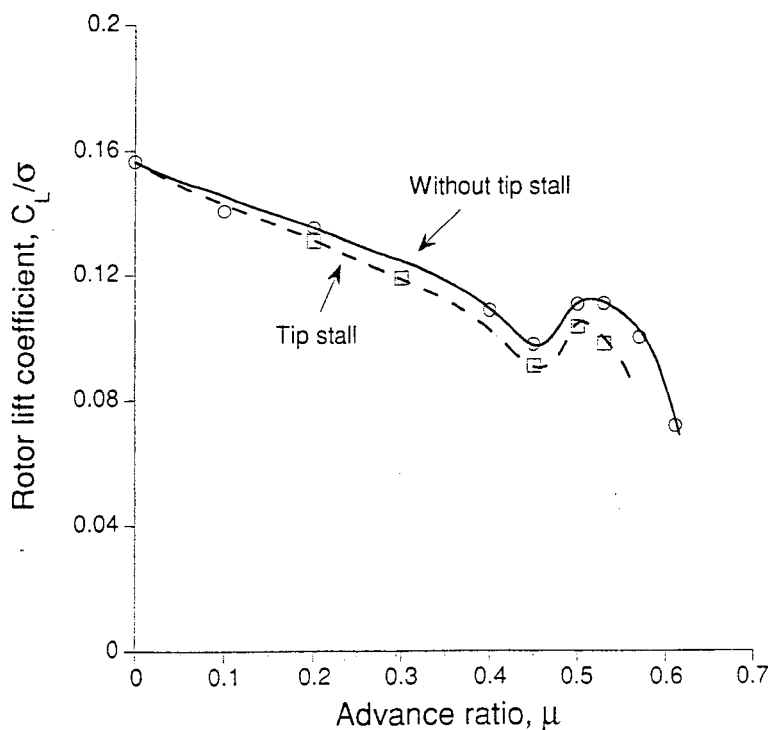
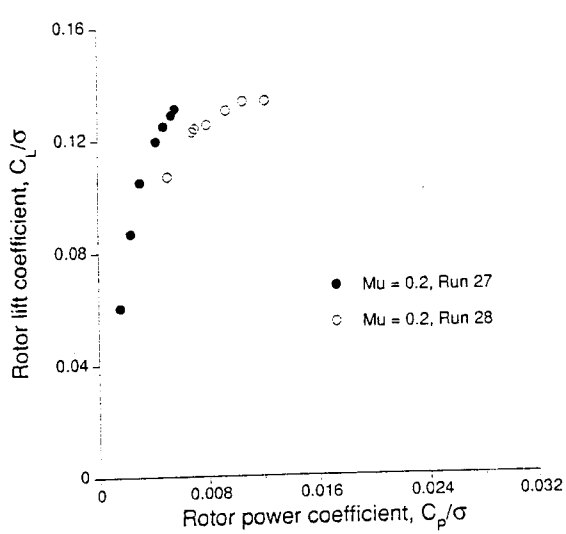
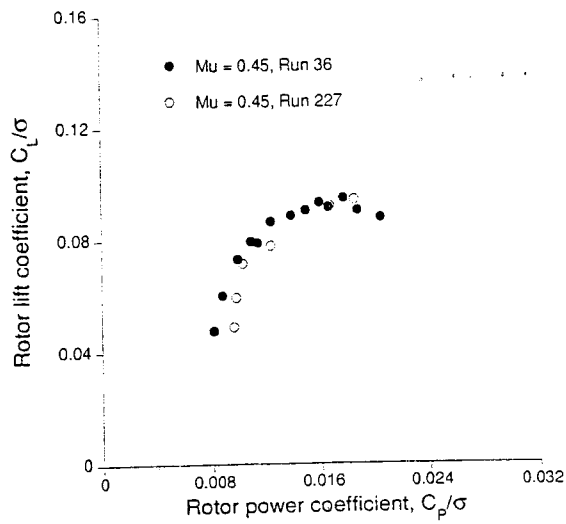


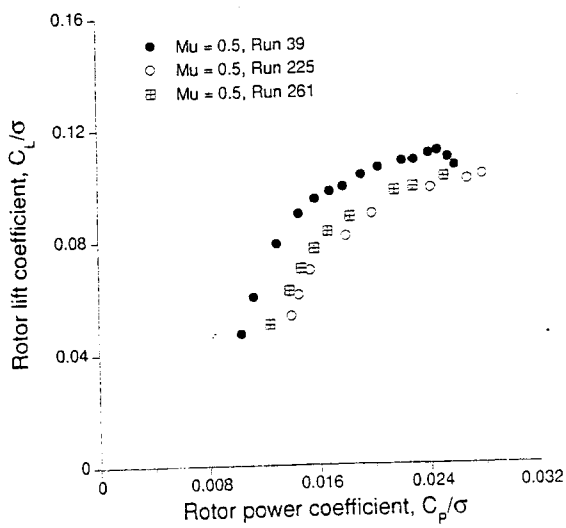
Fig. 1 Maximum lift limit measured from wind tunnel test



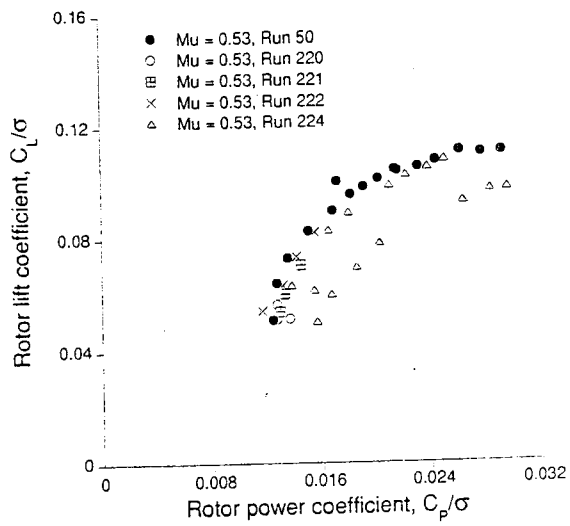
(a) $\mu = 0.2$



(b) $\mu = 0.45$



(c) $\mu = 0.5$



(d) $\mu = 0.53$

Fig. 2 Rotor lift versus power, $X/qd^2\sigma = 0.05$, shows all advance ratios with repeat conditions.

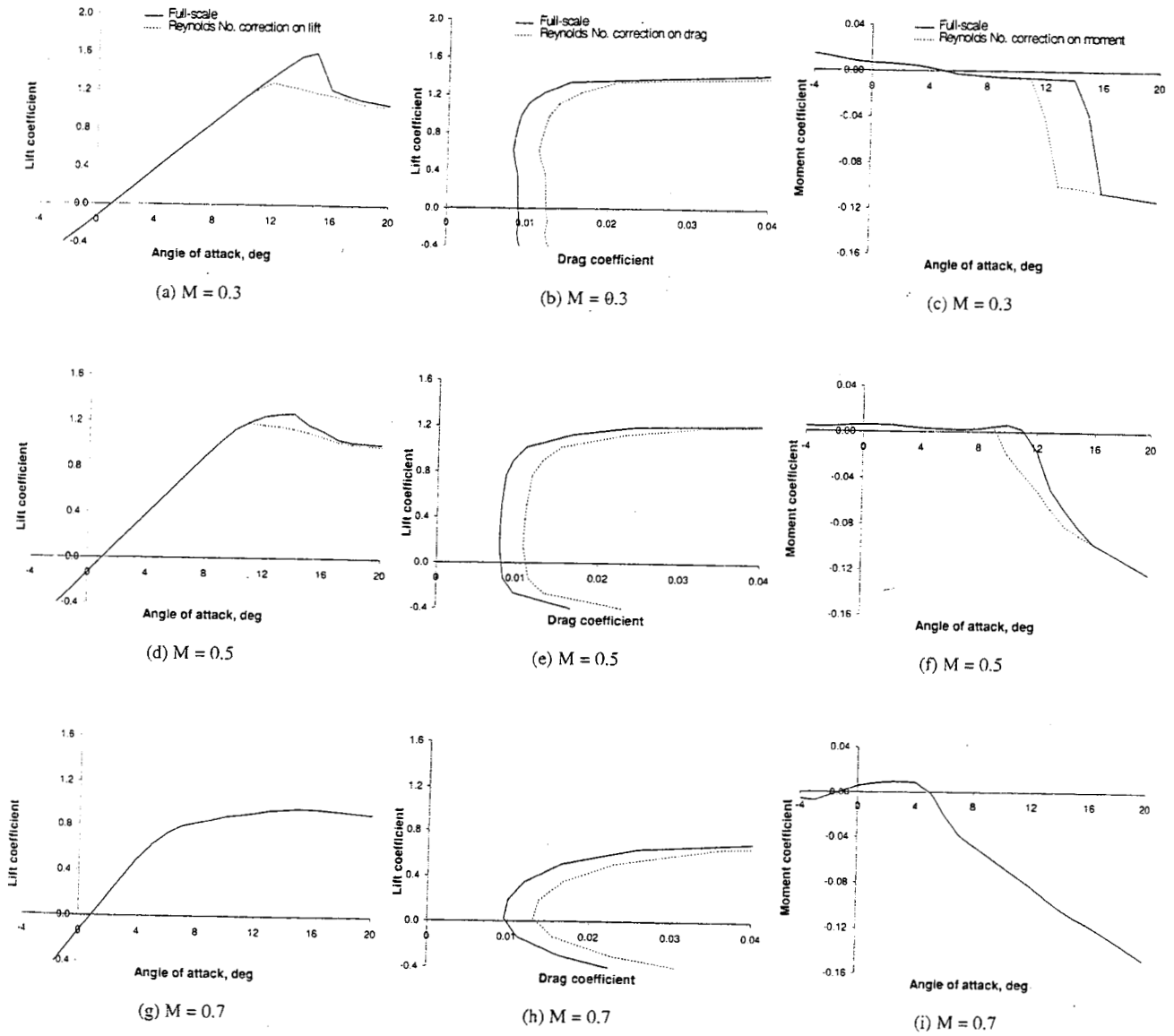


Fig. 3 Airfoil Characteristics

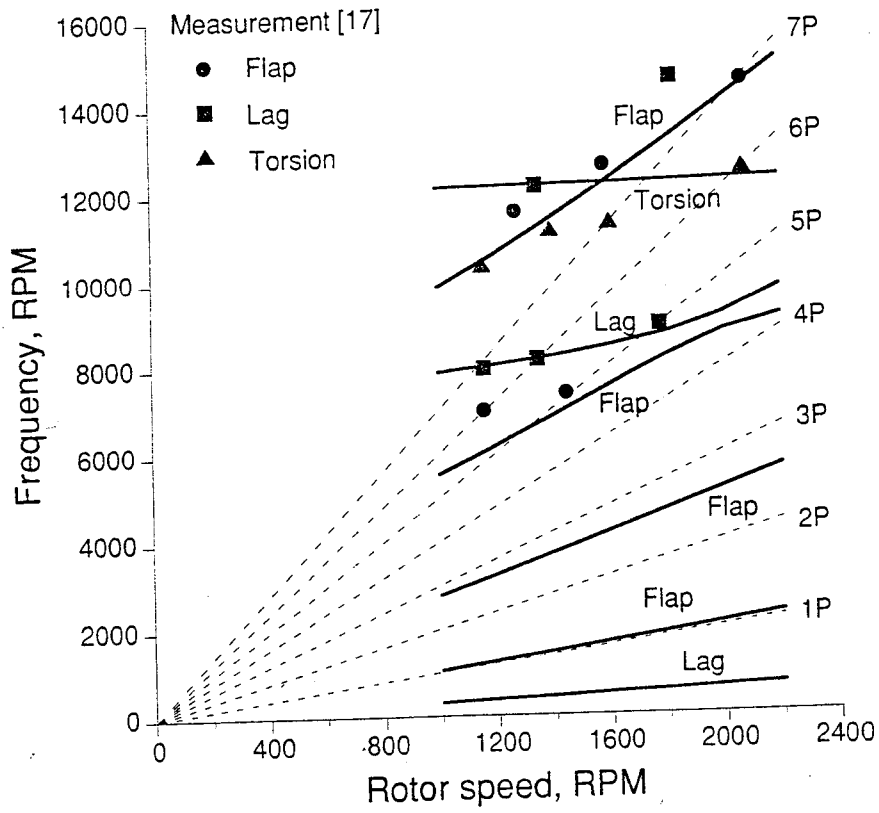
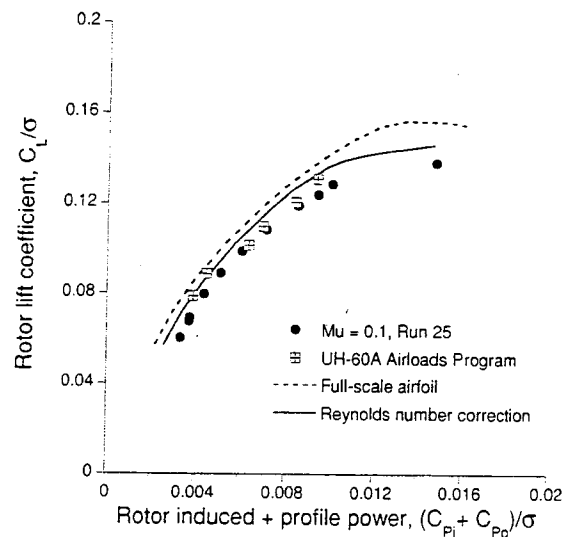
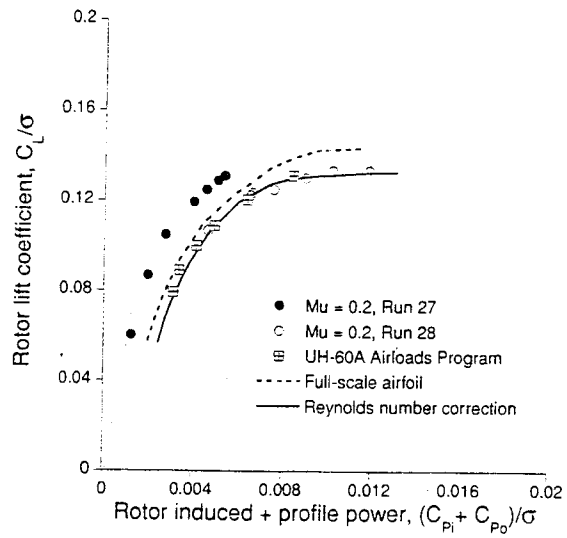


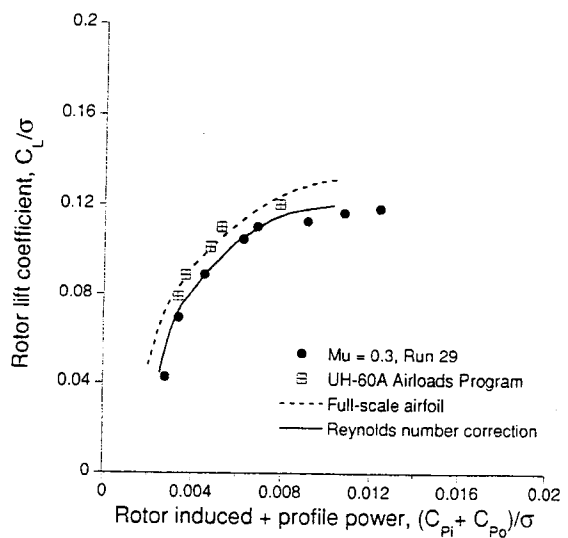
Fig. 4 Blade natural frequency



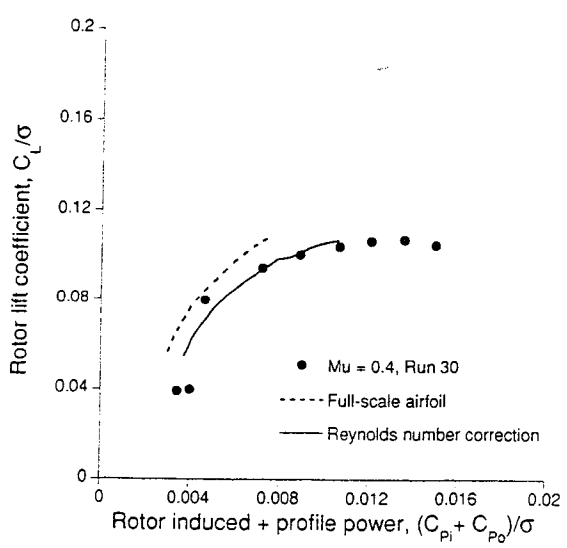
(a) $\mu = 0.1$



(b) $\mu = 0.2$



(c) $\mu = 0.3$



(d) $\mu = 0.4$

Fig. 5 Effects of Reynolds number on calculated rotor performance

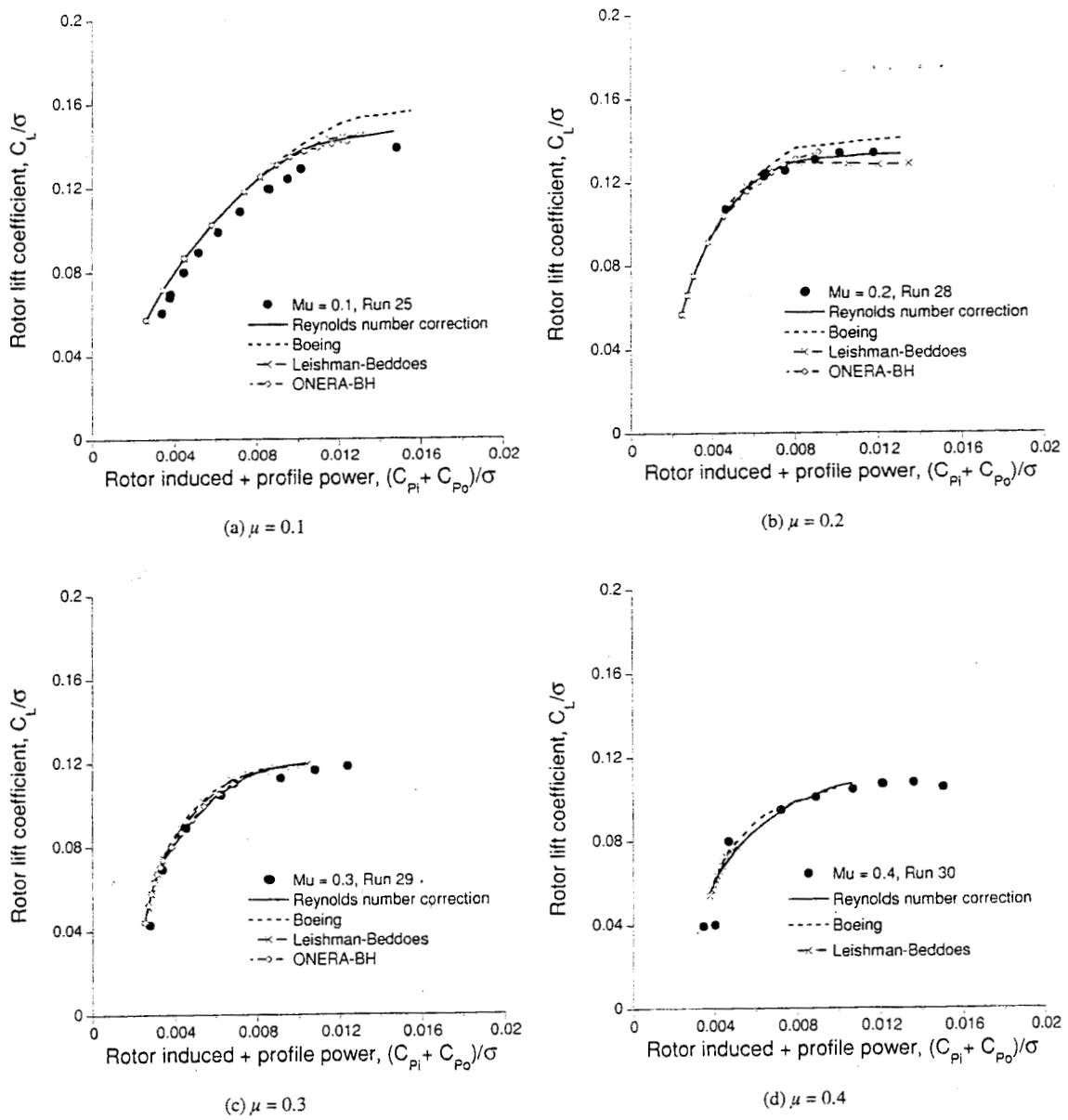


Fig. 6 Effects of dynamic stall models on rotor performance

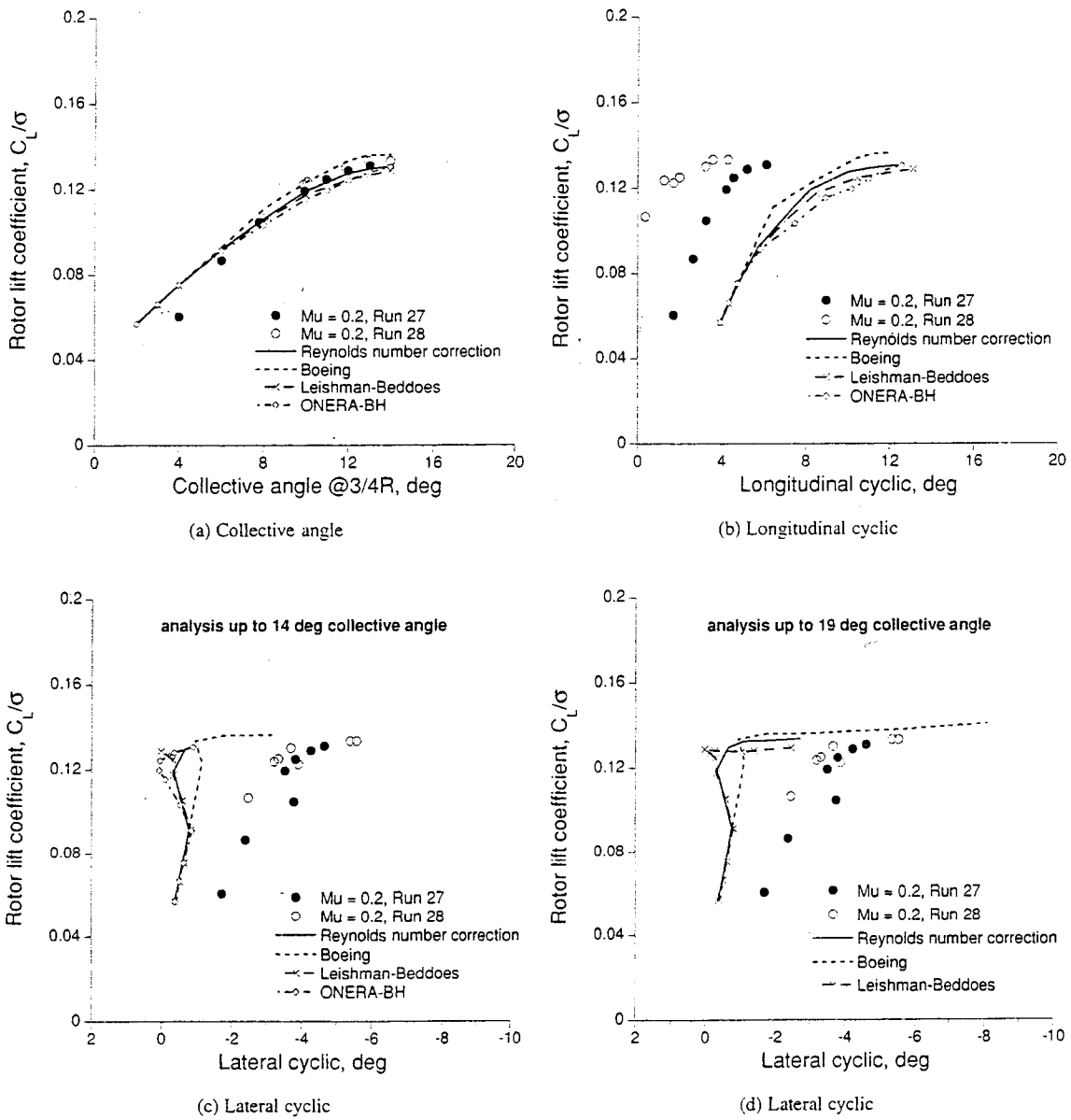
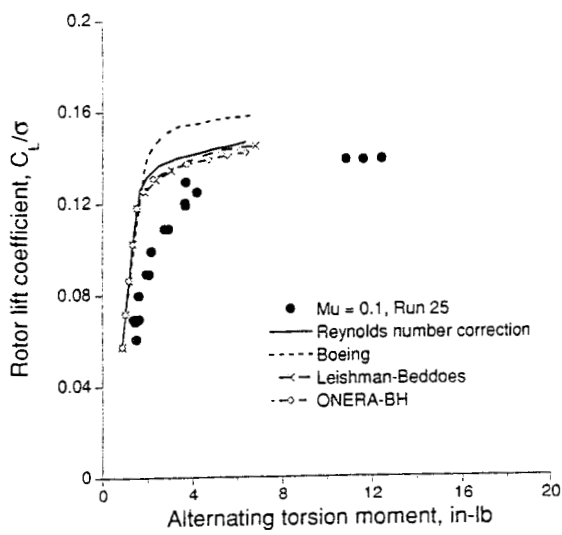
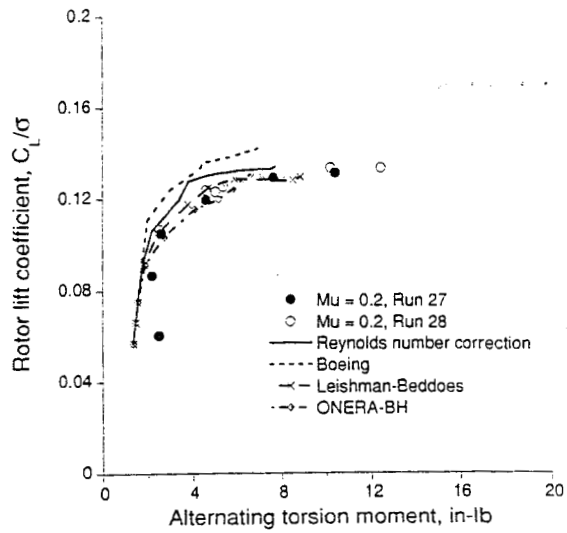


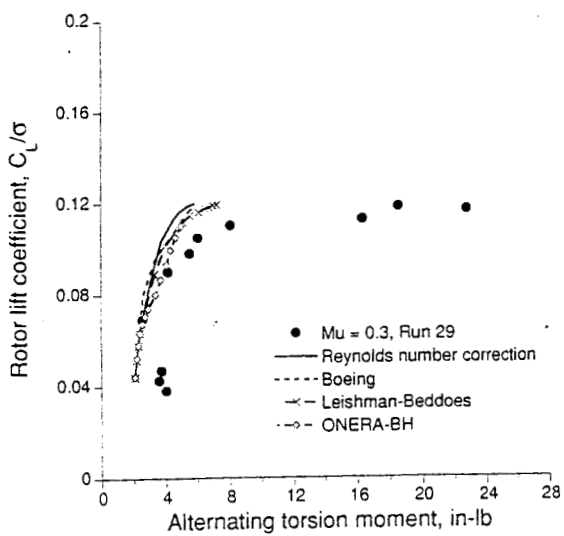
Fig. 7 Effects of dynamic stall models on rotor trim, $\mu = 0.2$



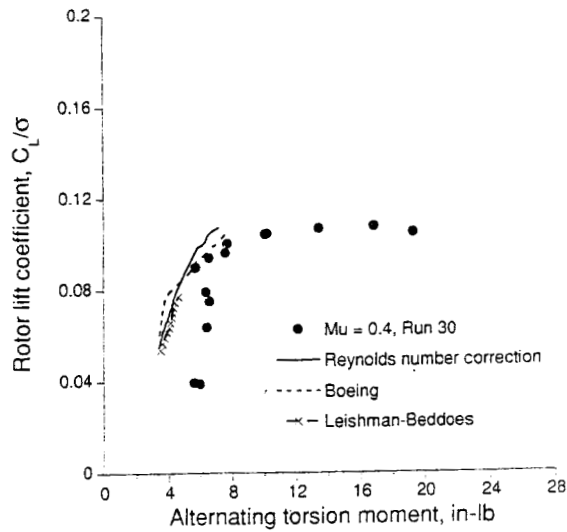
(a) $\mu = 0.1$



(b) $\mu = 0.2$

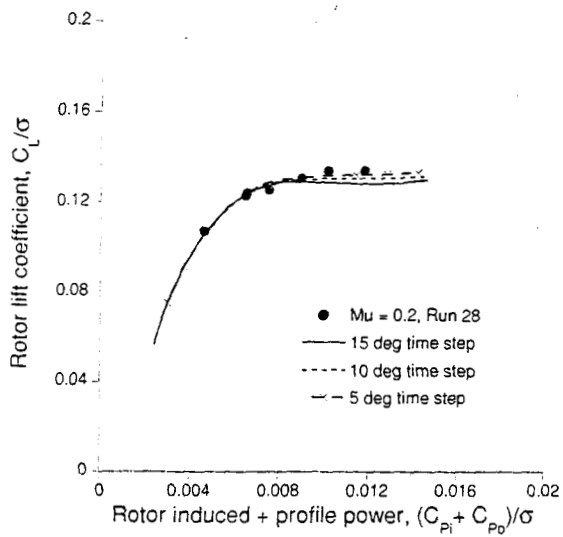


(c) $\mu = 0.3$

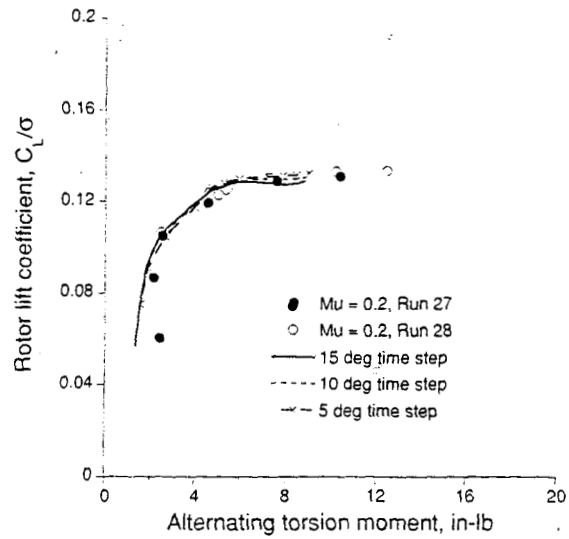


(d) $\mu = 0.4$

Fig. 8 Effects of dynamic stall models on torsion moment



(a) Rotor performance



(b) Alternating torsion moment @ 11.8%R

Fig. 9 Effects of time step on rotor performance and loads using the Leishman-Beddoes model at $\mu = 0.2$